

Simulation of inelastic-scattering contributions to the irradiance field in the ocean: variation in Fraunhofer line depths

Yuntao Ge, Howard R. Gordon, and Kenneth J. Voss

Raman scattering and fluorescence are important processes in oceanic optics because of their influence on the natural light field in the water. Monte Carlo simulations are described that verify that measurements of the Fraunhofer line depth in the in-water irradiance can be used to separate the irradiance into elastic and inelastic components, i.e., components that are generated by elastic- and inelastic-scattering processes, respectively. Specifically, the upwelling and downwelling irradiances, including Raman scattering, are simulated for a variety of model oceans. The inherent optical properties of the ocean are derived from a bio-optical model in which the elastic-scattering and the absorption coefficients of the biological material depend only on the phytoplankton pigment concentration, C . The Fraunhofer line at 656 nm is found to fill in, i.e., disappear into, the background continuum rapidly with increasing depth. This indicates a rapid transition from a near-surface light field dominated by elastic scattering to one composed of irradiance derived entirely from Raman scattering. Conversely the depth of the Fraunhofer line at 486 nm is nearly independent of depth in the water, indicating that Raman scattering never makes a significant contribution to the irradiance there. Between these two extremes, the lines at 518 and 589 nm show variations in line depths that depend significantly on C , e.g., at 518 nm the line fills in with increasing depth at low- C values but not at high- C values.

Introduction

Inelastic processes have become of more interest in oceanic optics since it was demonstrated that Raman scattering can play a significant role in radiative transfer in the upper layers of the water column,¹⁻³ and that they may also contribute to the radiance leaving the sea surface and thus influence the signal available for remote sensing in the visible.⁴ Fluorescence, another inelastic process, has long been known to contribute to the light field in the red near 685 nm by virtue of the chlorophyll a pigment contained in marine phytoplankton.^{5,6} Additionally it has been suggested that fluorescence in the blue-green of dissolved organic matter in the sea can also contribute to the radiance leaving the ocean surface.⁷

In the case of chlorophyll a fluorescence, its contribution to the total in-water light field near 685 nm is evident by its distinct spectral signature. The contribution of Raman scattering to the in-water light field

has been estimated from model computations based on the Raman-scattering cross section of water determined in the laboratory. In contrast, dissolved organic matter fluorescence is a broadband emission that varies with both the nature and with the concentration of the fluorescing compounds, and therefore its contribution to the light field cannot be determined by a distinct spectral signature or by radiative transfer modeling. It must be measured directly. Direct measurements of these inelastic processes in the water can be made by observing the filling in of Fraunhofer absorption lines in the solar spectrum.

The spectrum of solar irradiance incident upon the surface is not a continuum but instead contains sharp absorption lines, throughout the visible spectrum, caused by solar constituents. The depth and the widths of these lines vary, with the deepest having a center irradiance that is approximately 20% of the background irradiance and $\sim 1 \text{ \AA}$ (0.1 nm) wide. By making high spectral resolution measurements of the irradiance or radiance through these absorption lines and comparing the depth of the line with the continuum, broadband sources of inelastic scattering or fluorescence can be detected. This technique has been used in the atmosphere by Grainger and Ring⁸ to measure air glow. Plascyk⁹ has described an

The authors are with the Department of Physics, University of Miami, Coral Gables, Florida 33124.

Received 18 March 1992.

0003-6935/93/214028-09\$06.00/0.

© 1993 Optical Society of America.

airborne instrument that makes measurements of luminescence from sources such as tracer dyes and plant chlorophyll. This technique is particularly helpful when used *in situ* in the ocean. As described below, the measurements of the Fraunhofer line can be used to separate the elastically scattered irradiance from light that has been generated by inelastic processes, giving an indication of the importance of these processes in the natural light field. The measurements are made *in situ* with natural levels of illumination, so problems that are due to extrapolating measurements made on samples removed from the environment and subject to unnatural light or temperature conditions are avoided.^{10,11}

As a first step in the process of developing instrumentation for studying inelastic processes in the ocean, we have carried out simulations of the effect of Raman scattering on several Fraunhofer lines as a function of the optical properties of the water. The result of these simulations are reported in this paper.

Radiative Transfer Function

The radiative transfer equation, including general inelastic-scattering processes, can be formulated in a manner similar to the development by Gordon⁵ and Preisendorfer and Mobley⁶ of radiative transfer in fluorescent media. Consider an ocean that is vertically stratified. Construct a coordinate system in which the x and y axes are on the sea surface, and the z axis goes into the ocean. Let the direction of a unit vector ξ in space be specified by the angles θ and ϕ such that the components of ξ are $(\xi_x, \xi_y, \xi_z) = (\cos \phi \sin \theta, \sin \phi \sin \theta, \cos \theta)$. Then, if $L(z, \theta, \phi, \lambda)$ is the radiance of wavelength λ at depth z traveling in a direction specified by θ and ϕ , the radiative transfer equation, including inelastic-scattering processes, is given by

$$\begin{aligned} \cos \theta \frac{dL(z, \theta, \phi, \lambda)}{dz} &= -c(z, \lambda)L(z, \theta, \phi, \lambda) \\ &+ \int_{\Omega'} \beta(z, \theta', \phi' \rightarrow \theta, \phi, \lambda)L(z, \theta', \phi', \lambda)d\Omega' \\ &+ \int \int_{\Omega'} \beta_{in}(z, \theta', \phi' \rightarrow \theta, \phi, \lambda_e \rightarrow \lambda) \\ &\times L(z, \theta', \phi', \lambda_e)d\Omega'd\lambda_e. \end{aligned} \quad (1)$$

In Eq. (1), $\beta(z, \theta', \phi' \rightarrow \theta, \phi, \lambda)$ is the volume scattering function describing the elastic scattering of radiance of wavelength λ from direction (θ', ϕ') to direction (θ, ϕ) . Similarly, $\beta_{in}(z, \theta', \phi' \rightarrow \theta, \phi, \lambda_e \rightarrow \lambda)$ is the volume scattering function for inelastic scattering. It describes the scattering of a photon of wavelength λ_e (here and below the subscript e stands for excitation) traveling in a direction (θ', ϕ') into a photon of wavelength λ traveling in a direction (θ, ϕ) . $c(z, \lambda)$ is the beam attenuation coefficient for all processes at

wavelength λ , i.e.,

$$c(z, \lambda) = a(z, \lambda) + b(z, \lambda) + b_{in}(z, \lambda \rightarrow \lambda'), \quad (2)$$

where $a(z, \lambda)$ is the absorption coefficient for photons of wavelength λ , and $b(z, \lambda)$ and $b_{in}(z, \lambda \rightarrow \lambda')$ are the total scattering coefficients for elastic and inelastic processes, respectively, and are given by

$$\begin{aligned} b(z, \lambda) &= \int_{\Omega'} \beta(z, \theta', \phi' \rightarrow \theta, \phi, \lambda)d\Omega', \\ b_{in}(z, \lambda \rightarrow \lambda') &= \int_{\Omega'} \beta_{in}(z, \theta', \phi' \rightarrow \theta, \phi, \lambda \rightarrow \lambda')d\Omega'. \end{aligned}$$

Typically, β and β_{in} depend on only the angle α between the directions (θ', ϕ') and (θ, ϕ) so

$$\begin{aligned} b(z, \lambda) &= 2\pi \int_0^\pi \beta(z, \alpha, \lambda) \sin \alpha d\alpha, \\ b_{in}(z, \lambda \rightarrow \lambda') &= 2\pi \int_0^\pi \beta_{in}(z, \alpha, \lambda \rightarrow \lambda') \sin \alpha d\alpha. \end{aligned}$$

In contrast to β , which is strongly peaked in the forward direction ($\alpha = 0$),¹² β_{in} is roughly isotropic for both fluorescence and Raman scattering, and therefore it is feasible to expand it in a series of Legendre polynomials, i.e.,

$$\beta_{in}(z, \alpha, \lambda_e \rightarrow \lambda) = \frac{1}{4\pi} \sum_{l=0}^N b_{in}^{(l)}(z, \lambda_e \rightarrow \lambda) P_l(\cos \alpha). \quad (3)$$

$N = 0$ for isotropically emitted fluorescence and $N = 2$ for Raman scattering.

In this paper we are interested in deriving the irradiances that are due to inelastic processes. The downwelling, upwelling, and scalar irradiances, respectively, are given by

$$\begin{aligned} E_d(z, \lambda) &= \int_0^{2\pi} \int_0^{\pi/2} \cos \theta L(z, \theta, \phi, \lambda) \sin \theta d\theta d\phi, \\ E_u(z, \lambda) &= - \int_0^{2\pi} \int_{\pi/2}^\pi \cos \theta L(z, \theta, \phi, \lambda) \sin \theta d\theta d\phi, \\ E_0(z, \lambda) &= \int_0^{2\pi} \int_0^\pi L(z, \theta, \phi, \lambda) \sin \theta d\theta d\phi. \end{aligned} \quad (4)$$

These can all be derived from the azimuthally averaged radiance:

$$L^{(0)}(z, \theta, \lambda) = \frac{1}{2\pi} \int_0^{2\pi} L(z, \theta, \phi, \lambda) d\phi.$$

Thus we shall average Eq. (1) over ϕ and work only with $L^{(0)}$. Inserting Eq. (3) into Eq. (1), using the spherical harmonic addition theorem, and averaging

over ϕ , we have

$$\begin{aligned} \cos \theta \frac{dL^{(0)}(z, \theta, \lambda)}{dz} &= -c(z, \lambda)L^{(0)}(z, \theta, \lambda) \\ &+ \int_{\Omega'} \beta^{(0)}(z, \theta' \rightarrow \theta, \lambda)L^{(0)}(z, \theta', \lambda)\sin \theta' d\theta' + J_{in}(z, \theta, \lambda), \end{aligned} \quad (5)$$

where

$$\beta^{(0)}(z, \theta' \rightarrow \theta, \lambda) = \frac{1}{2\pi} \int_0^{2\pi} \beta(z, \theta', \phi' \rightarrow \theta, \phi, \lambda) d\phi,$$

and J_{in} , the source function for inelastic processes, is given by

$$J_{in}(z, \theta, \lambda) = \frac{1}{4\pi} \sum_{l=0}^N \int b_{in}^{(l)}(z, \lambda_e \rightarrow \lambda) P_l(\cos \theta) E_l(z, \lambda_e) d\lambda_e, \quad (6)$$

with

$$E_l(z, \lambda_e) = 2\pi \int_0^\pi P_l(\cos \theta') L^{(0)}(z, \theta', \lambda_e) \sin \theta' d\theta'. \quad (7)$$

We note that E_l for $l = 0$ is just the scalar irradiance at λ_e , while E_l for $l = 1$ is the net or vector irradiance $E_d - E_u$ at λ_e , etc. Equations (5)–(7) show that the inelastic component of the irradiance at λ depends on only the irradiances [Eq. (7)] at the excitation wavelength(s) and on the $b^{(l)}$ coefficients for the particular process.

For the two processes we are concerned with here, fluorescence and Raman scattering, it is easy to write down $b_{in}^{(l)}$. For isotropic fluorescence, $b_{in}^{(l)} \equiv b_{fl}^{(l)}$ and $b_{fl}^{(l)} = 0$ for $l \neq 0$, while $b_{fl}^{(0)}(z, \lambda_e \rightarrow \lambda) = b_{fl}(z, \lambda_e \rightarrow \lambda)$. Therefore the fluorescence source function, $J_{fl}(z, \theta, \lambda)$, is

$$J_{fl}(z, \theta, \lambda) = \frac{1}{4\pi} \int b_{fl}(z, \lambda_e \rightarrow \lambda) E_0(z, \lambda_e) d\lambda_e. \quad (8)$$

For Raman scattering, $\beta_{in} \equiv \beta_r$, and the angular distribution of β_r is given by¹³

$$\begin{aligned} \beta_r(z, \alpha, \lambda_e \rightarrow \lambda) &= \frac{3}{16\pi} \left(\frac{1+3\rho}{1+2\rho} \right) (1 + \gamma \cos^2 \alpha) b_r(z, \lambda_e \rightarrow \lambda) \\ &= \frac{3}{16\pi} \left(\frac{1+3\rho}{1+2\rho} \right) \left[1 + \frac{1}{3} \gamma + \frac{2}{3} \gamma P_2(\cos \alpha) \right] b_r(z, \lambda_e \rightarrow \lambda), \end{aligned}$$

where

$$\gamma = \frac{1 - \rho}{1 + 3\rho}$$

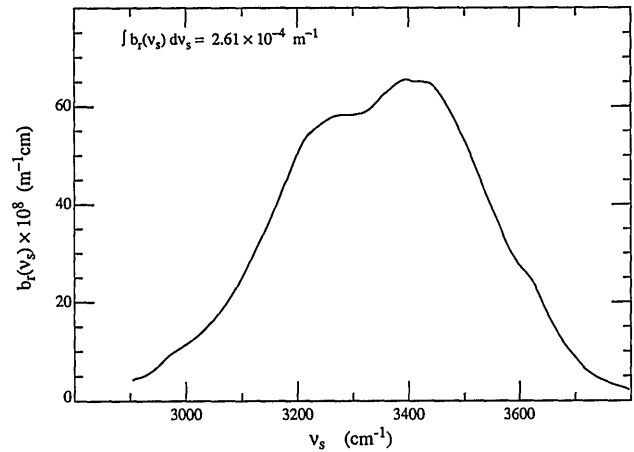


Fig. 1. Raman-scattering coefficient as a function of the Raman shift, ν_s .

and ρ is the depolarization ratio. Thus,

$$\begin{aligned} b_r^{(0)}(z, \lambda_e \rightarrow \lambda) &= b_r(z, \lambda_e \rightarrow \lambda), \\ b_r^{(2)}(z, \lambda_e \rightarrow \lambda) &= \frac{1}{2} \left(\frac{1 - \rho}{1 + 2\rho} \right) b_r(z, \lambda_e \rightarrow \lambda). \end{aligned}$$

All the other $b_r^{(l)}$'s are 0. Finally, the source function for Raman scattering, $J_r(z, \theta, \lambda)$, is given by

$$\begin{aligned} J_r(z, \theta, \lambda) &= \frac{1}{4\pi} \int b_r(z, \lambda_e \rightarrow \lambda) E_0(z, \lambda_e) \\ &\times \left[1 + \frac{1}{2} \left(\frac{1 - \rho}{1 + 2\rho} \right) \frac{E_2(z, \lambda_e)}{E_0(z, \lambda_e)} P_2(\cos \theta) \right] d\lambda_e. \end{aligned} \quad (9)$$

For narrow-band excitation, e.g., from a laser, the Raman-scattered light from water occurs in a band that is shifted $\sim 3400 \text{ cm}^{-1}$ in wave number from the excitation. If ν_e is the wave number ($1/\lambda_e$) corresponding to the excitation and ν the wave number of the emission, then $\nu + \nu_s = \nu_e$, where ν_s is the Raman shift. Figures 1 and 2 provide $b_r(\nu_s)$ and $\rho(\nu_s)$, respec-

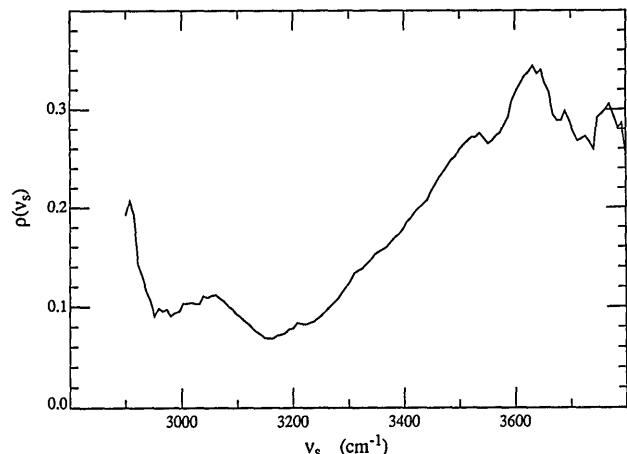


Fig. 2. Depolarization ratio as a function of ν_s for Raman scattering.

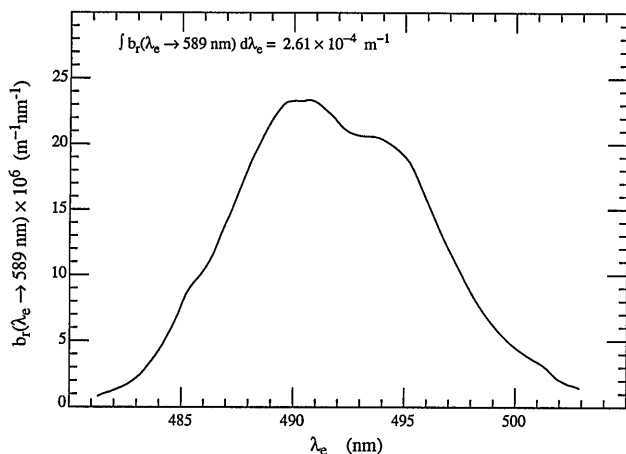


Fig. 3. Effective contribution of excitation wavelength λ_e to the Raman-scattered light in a narrow band around 589 nm. This shows that the source of the Raman-generated irradiance at the 589-nm Fraunhofer line is broad, approximately 25 nm in width.

tively, for pure water excited at 488 nm. They were prepared by combining the total Raman-scattering coefficient, $b_r = \int b_r(\nu_s) d\nu_s$, measured by Marshall and Smith³ with the spectral measurements of Chang and Young.¹⁴ When a narrow band of emission wave numbers is being examined the excitation can come from a band of wave numbers of the order of 500 cm^{-1} wide. For example, $b_r(\lambda_e \rightarrow \lambda)$, where $\lambda = 589 \text{ nm}$ as a function of λ_e is provided in Fig. 3.

Equations (5), (8), and (9) must be solved to predict the irradiances at λ resulting from inelastic processes. They show that in the case of fluorescence and Raman scattering, E_0 and E_2 are all that are required at the excitation wavelength to effect a solution.

Monte Carlo Simulation including Inelastic Processes

Gordon¹⁵ has developed an accurate Monte Carlo code for simulating the irradiances in the coupled ocean-atmosphere system. Vertical variations in all the inherent optical properties (IOP's) can be accommodated in the code.¹⁶ It employs a bio-optical model of Case 1 waters¹⁷ in which all the optical properties are related to phytoplankton pigment concentration C : the sum of the concentrations of chlorophyll a and its degradation product phaeophytin a . This model has recently been improved¹⁶ by separately specifying the scattering and the absorption properties of plankton and detrital particles. In the present work we simulate the excitation and emission separately. The existing code was used to simulate the standard excitation irradiances but was modified to provide $E_i(z, \lambda_e)$. The excitation irradiances then provide the photon source for the simulation at the emission wavelength through Eqs. (8) and (9).

At emission wavelength λ , the source function resulting from a narrow band of excitation wave-

lengths $\Delta\lambda_e$ is

$$J_{\text{in}}(z, \theta, \lambda) = \frac{1}{4\pi} b_{\text{in}}(z, \lambda_e \rightarrow \lambda) \Delta\lambda_e E_0(z, \lambda_e) \times \sum_{l=0}^N \frac{b_{\text{in}}^{(l)}(z, \lambda_e \rightarrow \lambda) E_l(z, \lambda_e)}{b_{\text{in}}(z, \lambda_e \rightarrow \lambda) E_0(z, \lambda_e)} P_l(\cos \theta),$$

where we have used the fact that $b_{\text{in}}^{(0)}(z, \lambda_e \rightarrow \lambda) = b_{\text{in}}(z, \lambda_e \rightarrow \lambda)$. We need to use this to inject inelastically scattered photons into the medium with the proper distribution in z and θ . This is straightforward, and it is easy to verify that z should be chosen from density $p(z)$, which is given by

$$p(z) = \frac{E_0(z, \lambda_e)}{\int_0^\infty E_0(z, \lambda_e) dz}; \quad (10)$$

so, given a random number r_j from the sequence $\dots r_j, r_{j+1}, r_{j+2}, \dots$, z is found from

$$r_j = \int_0^z p(z') dz'.$$

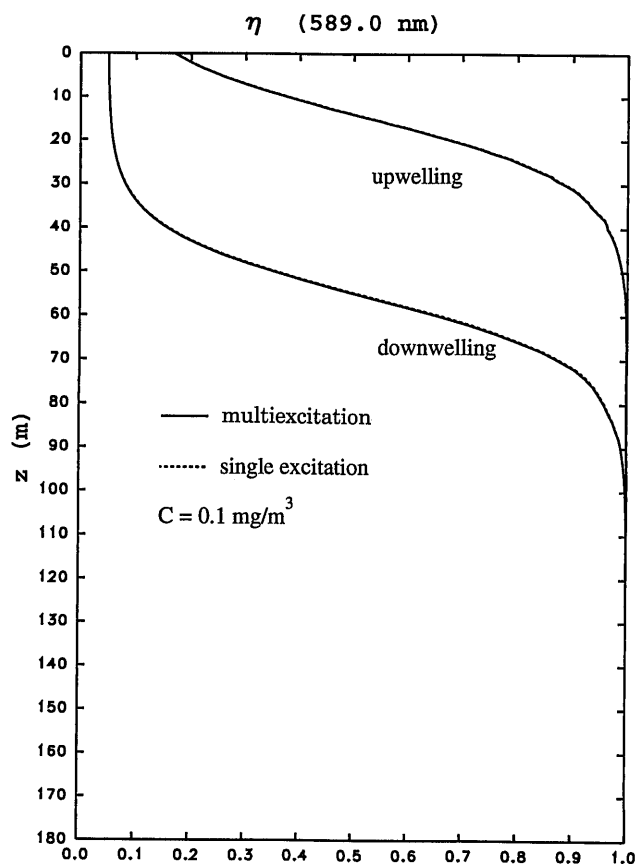


Fig. 4. Parameter η as a function of depth for the upwelling and downwelling irradiances. The multiexcitation case results from splitting the excitation into four equal portions with different depolarization ratios, excitation wavelengths, IOP's, and incident solar irradiances, and subsequently treats each portion separately. The single excitation example uses average properties for an excitation source at the center of the excitation band.

Given z , θ should be chosen from the conditional density $p(\theta|z)$, which is given by

$$p(\theta|z) = \frac{1}{4\pi} \sum_{l=0}^N \frac{b_{in}^{(l)}(z, \lambda_e \rightarrow \lambda) E_l(z, \lambda_e)}{b_{in}(z, \lambda_e \rightarrow \lambda) E_0(z, \lambda_e)} P_l(\cos \theta), \quad (11)$$

so

$$r_{j+1} = \int_0^\theta p(\theta'|z) d\theta'.$$

Finally, the weight of the emitted photon must be

$$W = b_{in}(z, \lambda_e \rightarrow \lambda) \Delta\lambda_e \int_0^\infty E_0(z, \lambda_e) dz, \quad (12)$$

so that $J_{in}(z, \theta, \lambda) = Wp(z)p(\theta|z)$, as required. Once a photon is emitted, it is followed in a manner similar to that which would be used in the absence of inelastic scattering with the exception that inelastic scattering from λ to longer wavelengths is included by increasing absorption coefficient $a(z, \lambda)$ by the appropriate inelastic-scattering coefficient, i.e., $b_{in}(z, \lambda \rightarrow \lambda')$ with $\lambda < \lambda'$. In our code, $E_0(z, \lambda_e)$ is normalized to unit irradiance at λ_e entering the top of the atmosphere, so the computed irradiances at λ are for unit irradiance

at λ_e entering the top of the atmosphere. They must be multiplied by the extraterrestrial solar irradiance, F_0 , to provide the actual irradiances. F_0 is taken from Neckel and Labs¹⁸ and averaged over the appropriate spectral intervals. This simulation technique can also be used with experimental measurements of E_l to predict the inelastically scattered irradiances for a given process, e.g., Raman scattering. Such measurements can be obtained by the use of instrumentation developed by Voss.^{19,20}

Fraunhofer Line Depth

It is helpful in describing the variation of the Fraunhofer lines to define a parameter η such that

$$\eta = \frac{E_f(\lambda)}{E_b(\lambda)},$$

where E_f is the irradiance at the center of a Fraunhofer line, and E_b is the irradiance of the background continuum. A similar definition could be made if one were interested in radiance as opposed to irradiance. With such a definition, $\eta = 0.2$ implies that the Fraunhofer line is very deep, i.e., $E_f = 0.2 E_b$, while $\eta = 1$ implies that the Fraunhofer line has totally disappeared, $E_f = E_b$.

The inelastic processes we are concerned with are

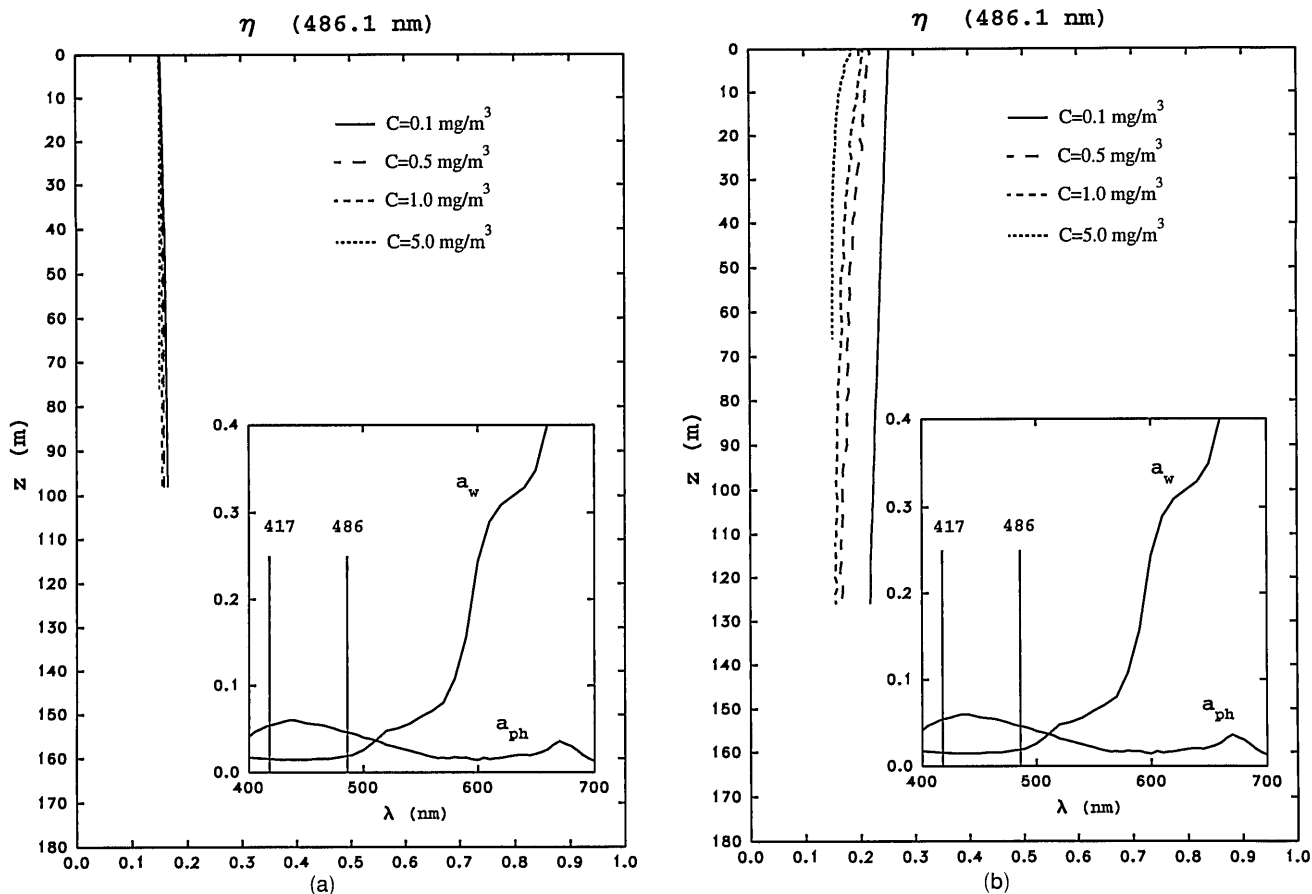


Fig. 5. Parameter η as a function of depth and pigment concentration for irradiance at the 486-nm Fraunhofer line. The downwelling case is shown in (a), while the upwelling case is shown in (b). The inset figure illustrates the absorption coefficient of water and phytoplankton ($C = 1 \text{ mg/m}^3$) in inverse meters, with the relevant excitation and emission lines.

broadband compared with the width of the Fraunhofer lines, so they will add irradiance to both the continuum and the Fraunhofer line equally. For example, as described earlier, Raman-scattered radiation is shifted approximately 3400 cm^{-1} and has a spectral width of approximately 500 cm^{-1} (Fig. 1). Thus the Raman line width is much larger than the typical spectral width of the Fraunhofer lines. Illumination of water with a narrow band of wavelengths near 537 nm results in a Raman line that is approximately 20 nm wide centered at the position of the C Fraunhofer line (656 nm), which has a width of $\sim 0.1\text{ nm}$.

As the inelastically generated irradiance grows to be a more significant proportion of the total irradiance, η will increase. The maximum η is, of course, unity and occurs when the irradiance is totally generated by inelastically processes. Using the value of η at a given depth combined with the value of η at the surface, one can separate the total irradiance into the inelastically scattered irradiance and the elastically scattered irradiance. At the surface, η is simply

$$\eta_s = \frac{E_{fs}(\lambda)}{E_{bs}(\lambda)},$$

where $E_{fs}(\lambda)$ and $E_{bs}(\lambda)$ are E_f and E_b for the downwelling irradiance just above the sea surface. By combining η_s with η at depth $\eta(z)$, several relation-

ships can be derived that show how the elastic (el) and inelastic (in) light fields can be separated. Simply,

$$E_d^{(in)}(z, \lambda) = \frac{\eta - \eta_s}{1 - \eta_s} E_d^{total}(z, \lambda),$$

$$E_d^{(el)}(z, \lambda) = \frac{1 - \eta}{1 - \eta_s} E_d^{total}(z, \lambda),$$

where $E_d^{total}(z, \lambda)$ is the irradiance in the background continuum, e.g., 1 nm away from the Fraunhofer line. Similar relationships can be derived for E_u .

Monte Carlo Results

Parameter η as a function of depth, pigment concentration, and wavelength was investigated using the techniques detailed above. b_r was taken³ to be $2.6 \times 10^{-4}\text{ m}^{-1}$ at 488 nm with a λ^{-5} dependence on wavelength.¹ If E_0 , E_2 , and ρ were independent of λ_e (or ν_e), they could be taken out of the integral in Eq. (9), and J_r would depend on only the total Raman-scattering coefficient, $b_r(\lambda) = \int b_r(\lambda_e \rightarrow \lambda) d\lambda_e$. The excitation for a given Fraunhofer line is broadband (Fig. 3), and the IOP's of the medium will vary across the excitation. This will cause E_0 , E_2 , and ρ to vary across the excitation band. To see if they vary sufficiently slowly with wavelength so that they can

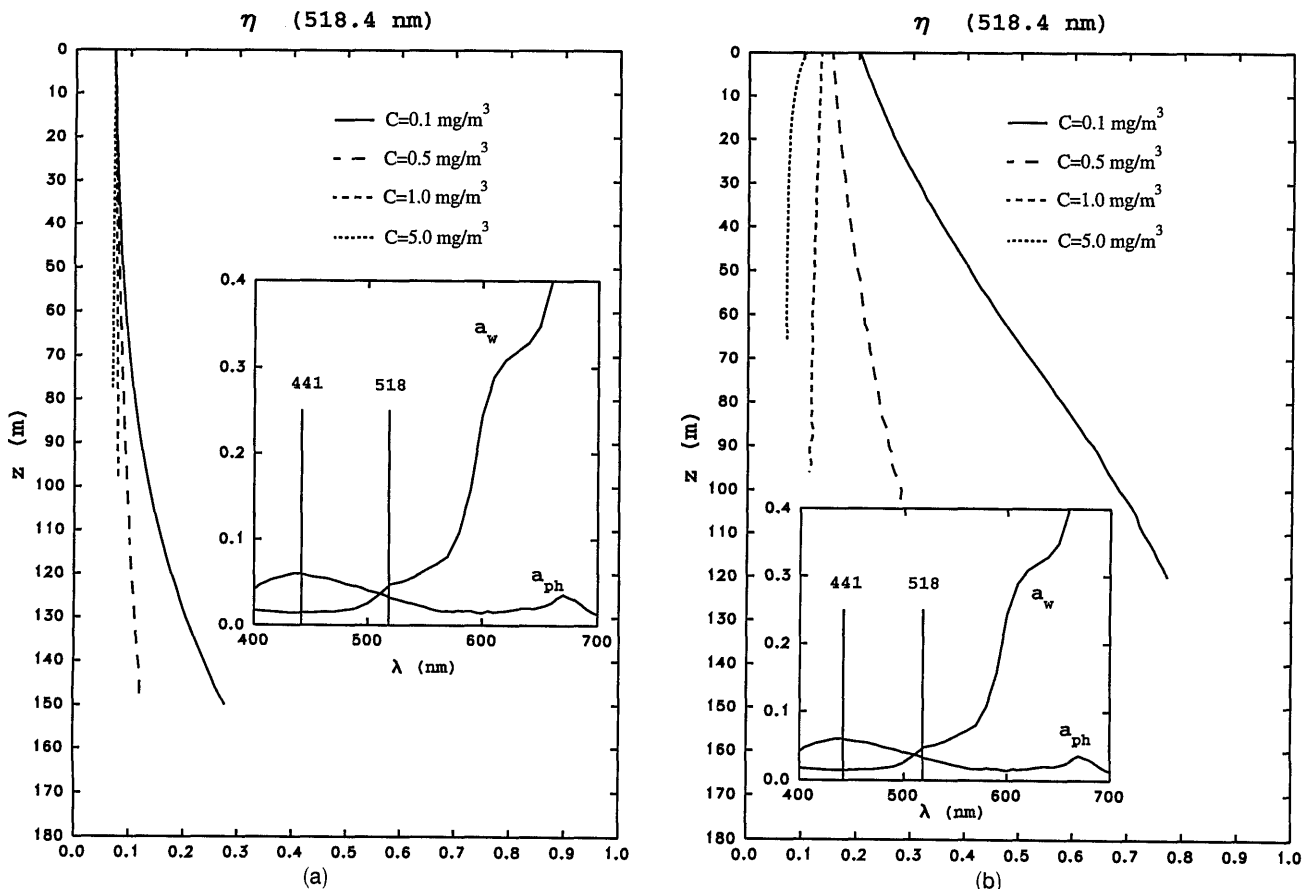


Fig. 6. As in Fig. 5, except at the 518-nm Fraunhofer line.

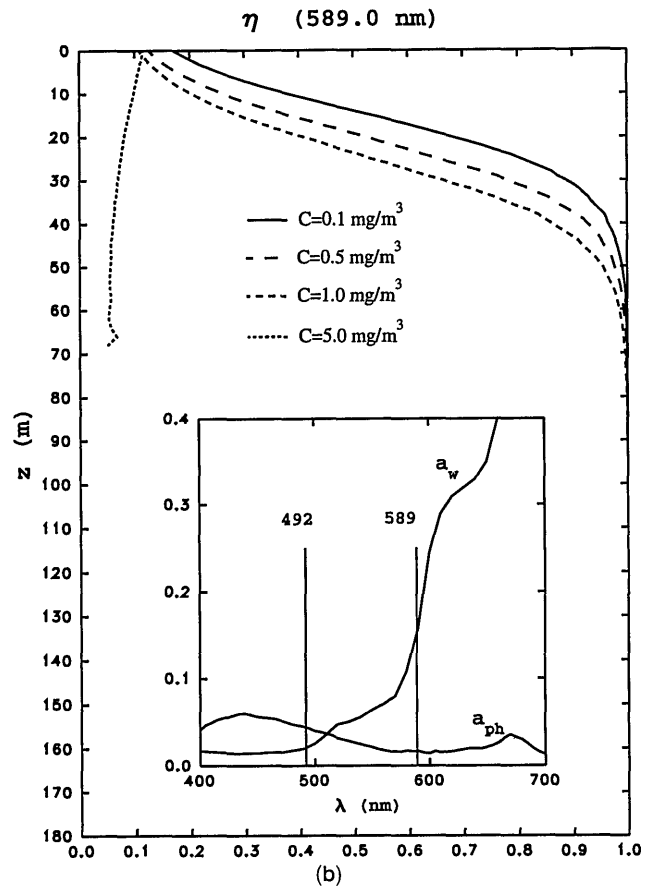
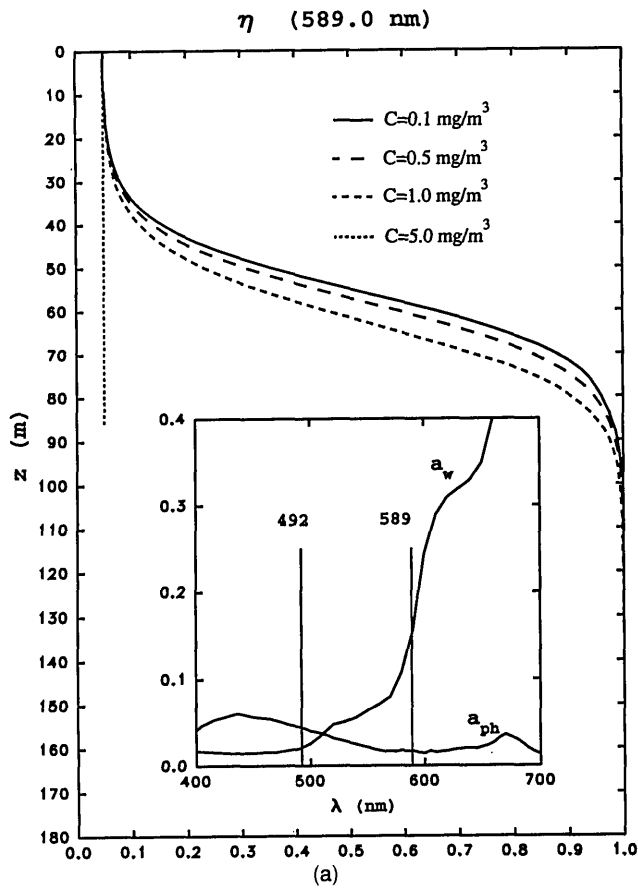


Fig. 7. As in Fig. 5, except at the 589-nm Fraunhofer line.

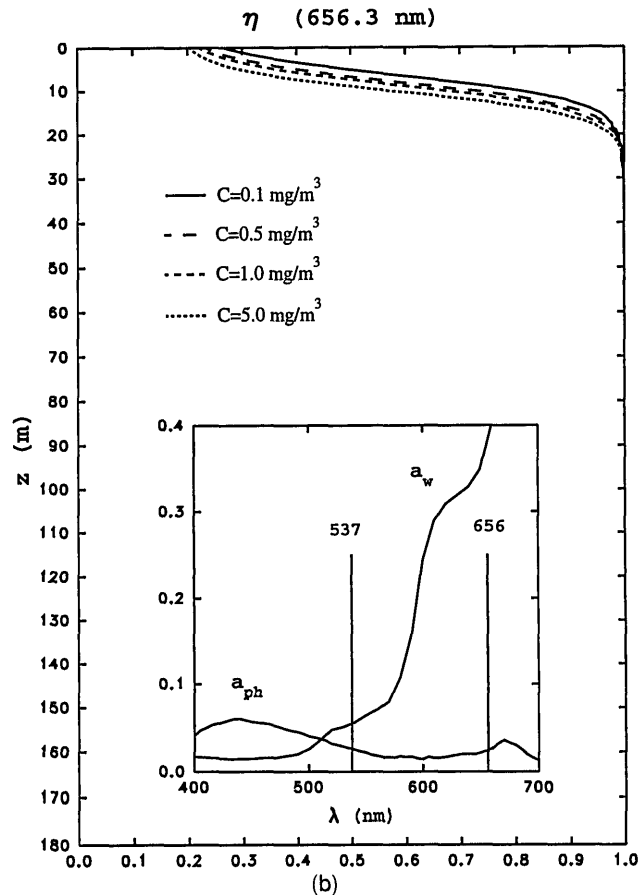
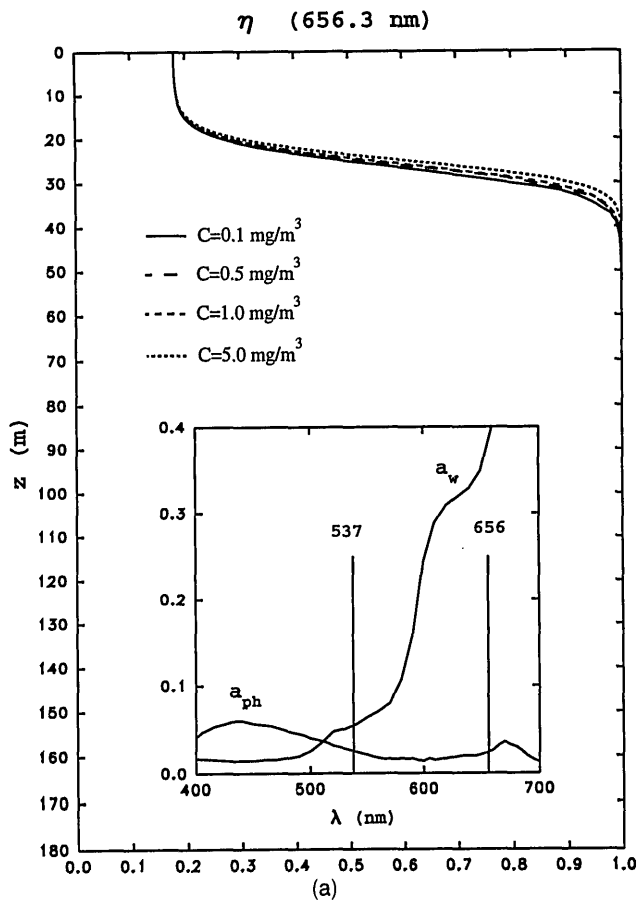


Fig. 8. As in Fig. 5, except at the 656-nm Fraunhofer line.

be replaced with spectral averages, we have examined η for the Fraunhofer line at 589 nm with a low pigment concentration ($C = 0.1 \text{ mg/m}^3$) in two ways. First, we used spectral averages of the IOP's over the entire excitation band and computed $\bar{\eta}$, the spectrally averaged source value. In an independent computation, the excitation (Fig. 3) was divided into four spectral bands, each of which contributes 25% to $b_r(\lambda)$. The Raman contribution of each of these bands was computed separately, and the results were summed to provide the total inelastic contribution, and, hence, η . $\bar{\eta}$ and η are compared in Fig. 4. Since the computationally intensive division of the excitation yields results that differ only slightly from $\bar{\eta}$, we utilize spectral averages (over the entire excitation band) in what follows. We also use the symbol η to stand for $\bar{\eta}$.

The computations of η for four Fraunhofer lines are plots shown in Figs. 5–8. Figures 5(a) and 5(b) illustrate the behavior for the Fraunhofer line at 486.1 nm. Figure 5(a) is for the downwelling irradiance, while Figure 5(b) is for the upwelling irradiance. The inset graph shows the excitation ($\lambda_e \sim 417 \text{ nm}$) and emission ($\lambda \sim 486 \text{ nm}$) wavelengths that are relevant for this Fraunhofer line, along with the spectral variation of the absorption coefficient for water and phytoplankton used in the model, specifically for $C = 1.0 \text{ mg/m}^3$. For the downwelling light field, η does not change significantly with depth or pigment concentration. This indicates that Raman scattering does not significantly influence the downwelling irradiance at this wavelength. In the upwelling light field there is a weak variation in η with depth and pigment concentration; however, it is clear that Raman scattering does not significantly influence E_u either. Figures 6(a) and 6(b) show the η parameter for the more interesting Fraunhofer line at 518 nm. In the downwelling irradiance field and at the lowest pigment concentration there is a depth dependence in η ; however, at higher concentrations it disappears. For the upwelling irradiance [Fig. 6(b)] there is a strong variation of η with depth at the lower pigment concentrations; however, at pigment concentrations above the lowest level, the depth dependence of η is small and, in fact, reverses, i.e., for low C , η increases with depth, but for high C , it decreases.

Figures 7(a) and 7(b) show η for the 589-nm Fraunhofer line. Here, η changes quickly at this wavelength from the surface value to 1. Remember that $\eta = 1$ implies that the light field is dominated by the inelastic processes, and that the Fraunhofer line has completely disappeared. Other than the highest pigment concentrations, η is strongly depth dependent. In Figs. 8(a) and 8(b), η for the 656-nm Fraunhofer line are displayed. In these figures it is obvious that the light field quickly becomes dominated by Raman scattering, regardless of pigment concentration.

The variation in η in these figures can be explained qualitatively by a simple model in which the behavior of η is determined by the relative magnitudes of the

attenuation coefficient for downwelling irradiance $K_d(\lambda)$ and upwelling irradiance $K_u(\lambda)$ at the excitation and the emission wavelengths. These are defined according to $K_d = -d \ln(E_d)/dz$ and $K_u = -d \ln(E_u)/dz$. A crude approximation¹⁵ for the K 's is that $K_u \approx K_d \sim a + b_b \approx a$, where a is the absorption coefficient and b_b is the backscattering coefficient. For the 656-nm line, K_d and K_u are much greater at the emission wavelength than at the excitation wavelength. Hence the elastically scattered and direct solar irradiance at the emission wavelength are attenuated rapidly, while the excitation source function is attenuated more slowly. The light field in this case quickly becomes dominated by the inelastically scattered light. Contrast this with 486 nm, where the K_d and K_u for the excitation and the emission irradiance fields are almost equal (see inset graph in Fig. 5). Here the direct and elastically scattered irradiances are attenuated at about the same rate as the emitted irradiance; hence, the Raman-generated irradiance can never dominate the light field. The behavior of E_u at 518 nm presents another interesting example [Fig. 6(b)]. At low- C values, the emission decays more rapidly than the excitation, while at high- C values the reverse is true. Thus η increases with depth for low C and decreases with depth at high C . This example provides an illustration of the transi-

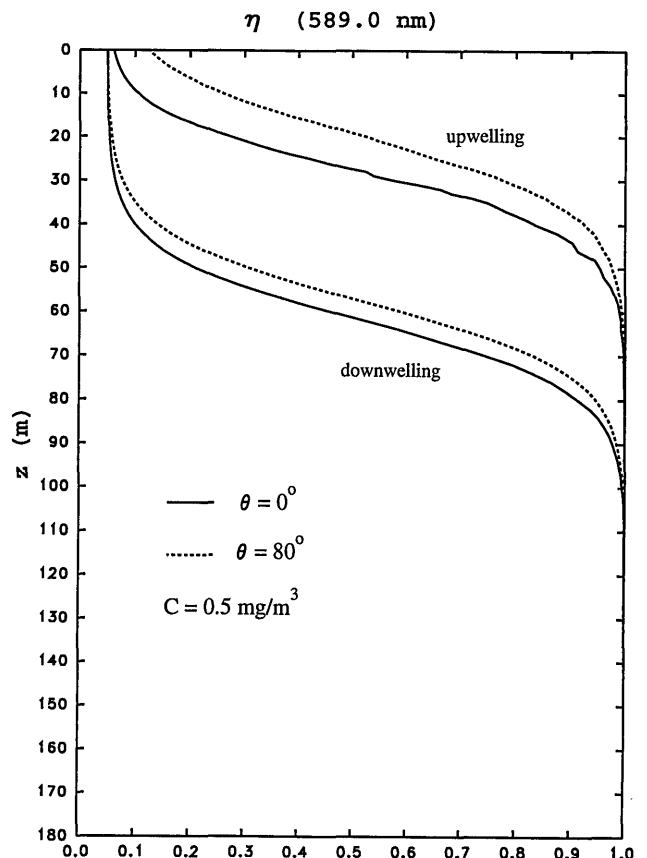


Fig. 9. Parameter η as a function of depth for the upwelling and the downwelling irradiances at the 589-nm Fraunhofer line for $C = 0.5 \text{ mg/m}^3$. This shows the variation of η with solar zenith angle θ_0 .

tion from inelastic to elastic domination as C increases.

The irradiance field depends on the surface illumination, so the depth variation of η will as well. Figure 9 illustrates an example of η for the upwelling and the downwelling irradiances for two extremes of sun zenith angles θ_0 , 0 and 80° , and for a pigment concentration of 0.5 mg/m^3 . The main effect of the sun angle is to increase the values of K_d and K_u with increasing solar zenith. This causes η to increase slightly faster at high values of θ_0 . However, one can see that the solar zenith angle should have a relatively weak effect on η .

Conclusion

Our model results have shown how Raman scattering will cause solar Fraunhofer lines to be filled at rates that depend on wavelength and pigment concentration. Clearly, by measuring the Fraunhofer lines in the ocean, we can gain information on the inelastic-scattering processes. Since there are Fraunhofer lines throughout the visible spectrum, instrumentation designed to measure them will enable the determination of the strength of inelastic-scattering processes throughout the visible and in varied water types. We are constructing a high-spectral resolution radiometer to measure η for various Fraunhofer lines throughout the visible, and our plan is to utilize Raman scattering to validate the methodology. We will then use the instrument to study the contribution of other inelastic processes to the light field. For the validation, we will directly measure the radiance distribution^{19,20} in the excitation band and use it to compute the profiles of E_0 and E_2 that are required for the Raman source function [Eq. (9)]. By measuring J_r directly, the accuracy of the bio-optical model at the excitation wavelength will not be an issue. The results here show that η is weakly dependent on C at 589 and 656 nm. These two Fraunhofer lines thus appear to be ideal for such a validation.

The authors are grateful to the U.S. Office of Naval Research, Ocean Optics Program, for providing support under grants N00014-89-J-1985 (H. R. Gordon) and N0014-90-J-1505 (K. J. Voss).

References

1. S. Sugihara, M. Kishino, and N. Okami, "Contribution of Raman scattering to upward irradiance in the sea," *J. Oceanogr. Soc. Jpn.* **40**, 397-404 (1984).
2. R. H. Stavn and A. D. Weidemann, "Optical modeling of clear ocean light fields: Raman scattering effects," *Appl. Opt.* **27**, 4002-4011 (1988).
3. B. R. Marshall and R. C. Smith, "Raman scattering and in-water ocean optical properties," *Appl. Opt.* **29**, 71-84 (1990).
4. R. H. Stavn, "Raman scattering effects at the shorter visible wavelengths in clear ocean water," in *Ocean Optics X*, R. W. Spinrad, ed., *Proc. Soc. Photo-Opt. Instrum. Eng.* **1302**, 94-100 (1990).
5. H. R. Gordon, "The diffuse reflectance of the ocean: The theory of its augmentation by chlorophyll a fluorescence at 685 nm," *Appl. Opt.* **18**, 1161-1166 (1979).
6. R. W. Preisendorfer and C. D. Mobley, "Theory of fluorescent irradiance fields in natural waters," *J. Geophys. Res.* **93D**, 10,831-10,855 (1988).
7. T. G. Peacock, K. L. Carder, C. O. Davis, and R. G. Steward, "Effects of fluorescence and water Raman scattering on models of remote sensing reflection," in *Ocean Optics X*, R. W. Spinrad, ed., *Proc. Soc. Photo-Opt. Instrum. Eng.* **1302**, 303-319 (1990).
8. J. F. Grainger and J. Ring, "Anomalous Fraunhofer line profiles," *Nature (London)* **193**, 762 (1962).
9. J. A. Plascyk, "The MK II Fraunhofer line discriminator (FLD II) for airborne and orbital remote sensing of solar stimulated luminescence," *Opt. Eng.* **14**, 339-346 (1975).
10. D. A. Kiefer, "Chlorophyll a fluorescence in marine centric diatoms: Responses of chloroplasts to light and nutrient stress," *Mar. Biol.* **22**, 39-46 (1973).
11. A. M. Kouassi, R. G. Zika, and J. M. C. Plane, "Light-induced alteration of the photophysical properties of dissolved organic matter in sea water," *Neth. J. Sea Res.* **27**, 33-41 (1990).
12. T. J. Petzold, "Volume scattering functions for selected natural waters," SIO Ref. 72-78 (Visibility Laboratory, Scripps Institution of Oceanography, San Diego, Calif., 1972).
13. S. P. S. Porto, "Angular dependence and depolarization ratio of the Raman effect," *J. Opt. Soc. Am.* **56**, 1585-1589 (1966).
14. C. H. Chang and L. A. Young, "Sea water temperature measurement from Raman spectra," Res. Note 960, N62269-73-C-0073 (Avco Everett Research Laboratory, Inc., sponsored by Advanced Research Projects Agency, ARPA order 2194, January 1974).
15. H. R. Gordon, "Can the Lambert-Beer law be applied to the diffuse attenuation coefficient of ocean water?" *Limnol. Oceanogr.* **34**, 1389-1409 (1989).
16. H. R. Gordon, "Diffuse reflectance of the ocean: Influence of nonuniform phytoplankton pigment profile," *Appl. Opt.* **31**, 2116-2129 (1992).
17. A. Morel and L. Prieur, "Analysis of variations in ocean color," *Limnol. Oceanogr.* **22**, 709-722 (1977).
18. H. Neckel and D. Labs, "The solar radiation between 3300 and 12500 Å," *Sol. Phys.* **90**, 205-258 (1984).
19. K. J. Voss, "Electro-optic camera system for measurement of the underwater radiance distribution," *Opt. Eng.* **28**, 241-247 (1989).
20. K. J. Voss, "Use of the radiance distribution to measure the optical absorption coefficient in the ocean," *Limnol. Oceanogr.* **34**, 1614-1622 (1989).